NANO LETTERS

2003
Vol. 3, No. 12
1625−1631

Spontaneous Polarization-Induced Nanohelixes, Nanosprings, and Nanorings of Piezoelectric Nanobelts

Xiang Yang Kong and Zhong Lin Wang*

School of Materials Science and Engineering, Georgia Institute of Technology, Atlanta, Georgia 30332-0245

Received July 1, 2003

ABSTRACT

Growth of (0001) facet-dominated, free-standing, piezoelectric zinc oxide (ZnO) nanostructures is challenged by the divergence of the surface energy due to intrinsic polarization. By controlling growth kinetics, we show the success of growing nanobelt-based novel structures whose surfaces are dominated by the polarized ±(0001) facets. Owing to the positive and negative ionic charges on the zinc- and oxygen-terminated ±(0001) surfaces, respectively, a spontaneous polarization is induced across the nanobelt thickness. As a result, right-handed helical nanostructures and nanorings are formed by rolling up single-crystal nanobelts; this phenomenon is attributed to a consequence of minimizing the total energy contributed by spontaneous polarization and elasticity. The polar-surface-dominated ZnO nanobelts are likely to be an ideal system for understanding piezoelectricity and polarization-induced ferroelectricity at nanoscale; and they could have applications as one-dimensional nanoscale sensors, transducers, and resonators.

Zinc oxide (ZnO) is a versatile smart material that has key applications in catalysts, sensors, piezoelectric transducers,[1] transparent conductors,[2] and surface acoustic wave devices.[3] The noncentral symmetry and the tetrahedral coordinated ZnO_4 unit in ZnO result in anisotropic piezoelectric properties. Structurally, the wurtzite structured ZnO crystal is described schematically as a number of alternating planes composed of four-fold coordinated O^{2-} and Zn^{2+} ions, stacked alternatively along the *c*-axis. The oppositely charged ions produce positively charged (0001)-Zn and negatively charged $(000\bar{1})$-O polar surfaces, resulting in a normal dipole moment and spontaneous polarization as well as a divergence in surface energy. To maintain a stable structure, the polar surfaces generally have facets or exhibit massive surface reconstructions, but ZnO ± (0001) is an exception, which is atomically flat, stable, and without reconstruction.[4,5] Understanding the superior stability of the ZnO ± (0001) polar surfaces is a forefront research in today's surface physics.[6−9]

Nanowire- and nanotube-based materials have been demonstrated as building blocks for nanocircuits, nanosystems,[10−14] and nanooptoelectronics,[15] and they have been fabricated for a wide range of materials from metals, semiconductors, and oxides to polymers.[16] A variety of quasi-one-dimensional ZnO nanostructures, such as nanowires[17] and nanobelts,[18] have been synthesized, and they have been used for fabricating nanoscale lasers,[17] field effect transistors,[19] gas sensors,[20] cantilevers,[21] and resonators.[22] But these ZnO nanostructures grow along the *c*-axis, and the side surfaces are $\{01\bar{1}0\}$ and $\{2\bar{1}\,\bar{1}0\}$ due to their energies which are lower than that of (0001), resulting in vanishing dipole moment and much reduced piezoelectricity. The most desirable morphology to maximize the piezoelectric effect is to create nanostructures that preserve large area (0001) polar surfaces.[23,24] However, ZnO (0001) has a surface energy that diverges with sample size due to the surface polarization charge. Therefore, *growth of (0001) surface-dominated free-standing nanostructures needs to overcome the barrier of surface energy.*

In this paper, we report the free-standing ZnO nanobelts that grow along the *a*-axis, and their large top and bottom surfaces are the polar (0001) facets. Due to the small thickness of the nanobelts, spontaneous polarization normal to the nanobelt leads to the growth of helical nanostructures. The mechanism for the helical growth is attributed to a consequence of minimizing the total energy contributed by spontaneous polarization and elasticity. The ZnO nanostructures have potential applications as nanoscale sensors, resonators, and transducers that could serve as functional components to be integrated in micro- and nanoelectromechanical systems (MEMS, NEMS). They are also ideal systems for understanding piezoelectric effect and spontaneous polarization induced ferroelectric effect at the nanoscale.

The structurally controlled, high-purity and high-yield ZnO nanobelts were synthesized by a solid−vapor process.[25] Zinc oxide powders (purity 99.99%, melting point 1975 °C) were

* Corresponding author. E-mail: zhong.wang@mse.gatech.edu.

10.1021/nl034463p CCC: $25.00
Published on Web 08/06/2003

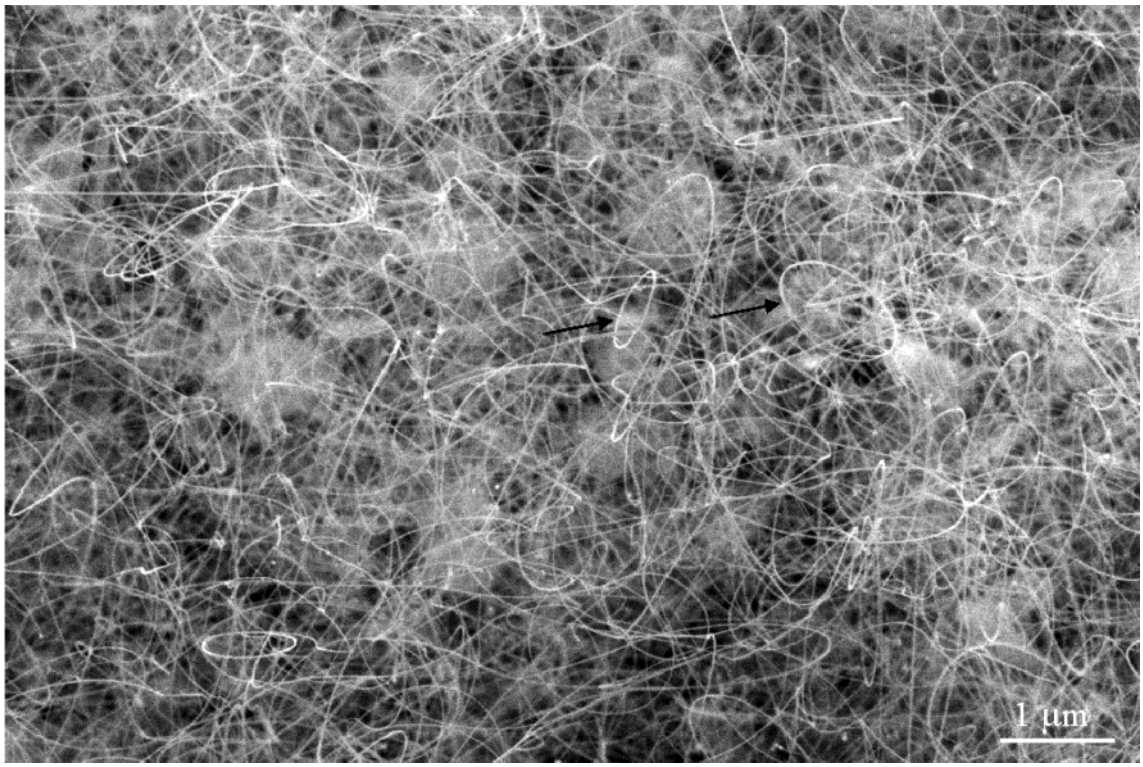

Figure 1. SEM images of the as-synthesized ZnO nanobelts, showing nanobelts of sizes 20−60 nm in widths and a large fraction of nanorings and helical nanostructures.

placed at the highest temperature zone of a horizontal tube furnace. Before heating to the desired temperature of 1350 °C, the tube furnace was evacuated to $\sim 10^{-3}$ Torr to remove the residual oxygen. Then the source materials were heated to 1350 °C at a heating rate of 20 °C/min. ZnO decomposes into Zn^{2+} and O^{2-} at high temperature (1350 °C) and low pressure ($\sim 10^{-3}$ Torr),[26] and this decomposition process is the key step for controlling the anisotropic growth of the nanobelts. After a few minutes of evaporation and decomposition, the Ar carrier gas was introduced at a flux of 25 sccm (standard cubic centimeters per minute). The synthesis process was conducted at 1350 °C for 30 min. The nanobelts were deposited onto an alumina substrate placed in a temperature zone of 400−500 °C under Ar pressure of 250 Torr. Structures of the ZnO nanobelts were analyzed by scanning electron microscopy (SEM) and high-resolution transmission electron microscopy (HRTEM).[27]

SEM and TEM analysis shows that the as-prepared product has a belt-shape with widths of 10−60 nm, thickness of 5−20 nm and lengths up to several hundreds of micrometers. The dominant component of the as-synthesized sample is nanobelts with a uniform size distribution, but a significant amount of nanobelts has ring shape (as indicated by arrowheads in Figure 1), which *has not been found for single-crystal nanobelts or nanowires of any other materials*.

The ZnO nanobelt has a controlled structure. By examining over hundreds of nanobelts laid down naturally onto a carbon film by electron diffraction (ED), more than 90% of them showed the same orientation of [0001] with respect to the incident electron beam (Figure 2A), indicating that the top flat surfaces of the nanobelts are the polar ±(0001) facets. This clearly demonstrates the success of overcoming the surface energy barrier by growth kinetics in achieving structural control. The ZnO nanobelt has a wurtzite structure with lattice constants of $a = 0.325$ nm and $c = 0.521$ nm. Indexing of the ED pattern shows that the nanobelt grows along $[2\bar{1}\bar{1}0]$ (the *a*-axis), with its top/bottom surface ±(0001) and the side surfaces $\pm(01\bar{1}0)$ (Figure 2B). HRTEM shows that the nanobelt is single crystalline without the presence of dislocations (Figure 2C), and its geometrical shape is uniform. The surfaces of the nanobelt are clean, atomically sharp and flat (Figure 2D). Due to the small thickness of 5−20 nm and large aspect ratio of ∼1:4, the flexibility and toughness of the nanobelts are extremely high so that it can be bent or twisted without fracture (Figure 2E,F). The crystallographic structural model of the nanobelt is presented in Figure 2G.

In addition to the significant portion of nanorings observed in Figure 1, the most striking feature of the sample is the formation of helical structures by rolling up single crystalline nanobelts (Figure 3).[25] The helical nanostructure has a uniform shape with radii of ∼500−800 nm and evenly distributed pitches. A nearly perfect circular arc is formed by a single nanobelt (Figure 4A). Electron diffraction indicates that the direction of the radius toward the center of the ring is always [0001] along the entire perimeter without significant twisting, and the circular plane of the nanoring is $[01\bar{1}0]$. A full circular ring formed by a closed nanobelt shows a consistent orientation (Figure 4B); the orientation of the straight or close-to-straight nanobelts is along [0001], in consistent to the result from Figure 2A. The orientation relationship presented in Figure 4A is preserved

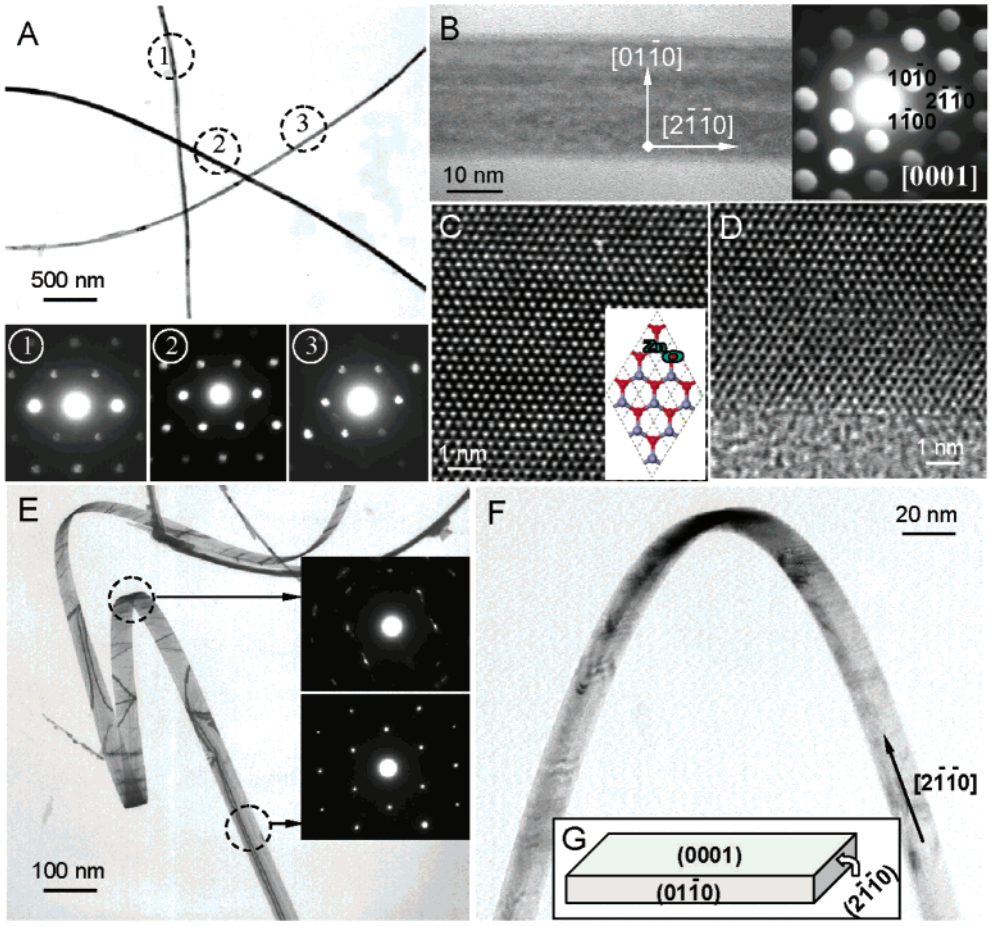

Figure 2. Controlled growth of (0001) polar-surface-dominated ZnO nanobelts. (A) Low-magnification TEM images and the corresponding electron diffraction patterns recorded from the areas as indicated by a sequence number from an TEM grid without tilting, showing their unanimous [0001] orientation on a flat carbon substrate. (B) TEM image and the corresponding electron diffraction pattern, showing that the nanobelt grows along [2$\bar{1}\bar{1}$0] (*a*-axis), with ±(0001) top and bottom surfaces, and ±(01$\bar{1}$0) side surfaces. (C) [0001] high-resolution TEM image recorded from the center of the nanobelt given in (B), showing its dislocation-free volume. The inset is the projected model of the wurtzite ZnO along [0001]; the positions of the Zn atoms are in correspondence to the white dots observed in the image. (D) [0001] profile high-resolution TEM image recorded from the edge of the nanobelt given in (B), showing the flatness of the surface. (E) Low magnification TEM image and the corresponding electron diffraction patterns recorded from the circled regions, displaying the geometry of the nanobelt. The difference between the two electron diffraction patterns is due to the bending in the local regions. The contrast observed in the image is the bending contour in electron imaging produced by the deformation of atomic planes. (F) TEM image showing the helical twist of a nanobelt. The dark contrast at the top is due to the local strain. (G) Structure model of the ZnO nanobelt.

for nanorings formed by double-looped (Figure 4C) and multiple-looped (Figure 4D) rolling of a nanobelt. The orientation of the two wider nanobelts across the nanoring in Figure 4C is [0001]. The enlarged images from the double-looped ring in Figure 4C clearly indicate that the two loops of the nanobelt are in physical contact, and there is even a small gap (∼1−2 nm, see the insets in Figure 4C) between them, suggesting that the interaction between the loops is weak and there is no chemical bonding. Overlap among the loops is possible for multiple-looped ring (see the inset in Figure 4D).

The (0001) plane can be terminated with Zn [(0001)-Zn] or oxygen [(000$\bar{1}$)-O], resulting in positively and negatively charged top and bottom surfaces, respectively. Convergent beam electron diffraction[28] has been applied to determine the polarity (Figure 4E), and the result indicates that the interior surface of the ring is (0001)-Zn and the exterior surface is (000$\bar{1}$)-O.[29] Physically, if the surface charges are uncompensated during the growth,[30] the net dipole moment tends to diverge and the electrostatic energy increases. For a thin nanobelt laying on a substrate, the spontaneous polarization induces electrostatic energy due to the dipole moment, but rolling up to form a circular ring would minimize or neutralize the overall dipole moment, reducing the electrostatic energy. On the other hand, bending of the nanobelt produces elastic energy. The stable shape of the nanobelt is determined by the minimization of the total energy contributed by spontaneous polarization and elasticity.

An analytical estimation of the total energy is given below. A nanobelt with spontaneous polarization and charge on the top and bottom surfaces can be approximated to be a capacitor. For simplicity, we propose a model in which a flat planar capacitor (length L, width W, and thickness t) is rolled up to form a cylindrical capacitor (inner radius R_1, outer radius R_2, and mean radius $R = (R_1 + R_2)/2$), as shown in Figure 4F. If the thickness of the nanobelt is much smaller than the mean radius of the cylinder ($t \ll R$, and $L = 2\pi R$) (typically $t \sim 10$ nm, $R \sim 500$ nm), the surface charge

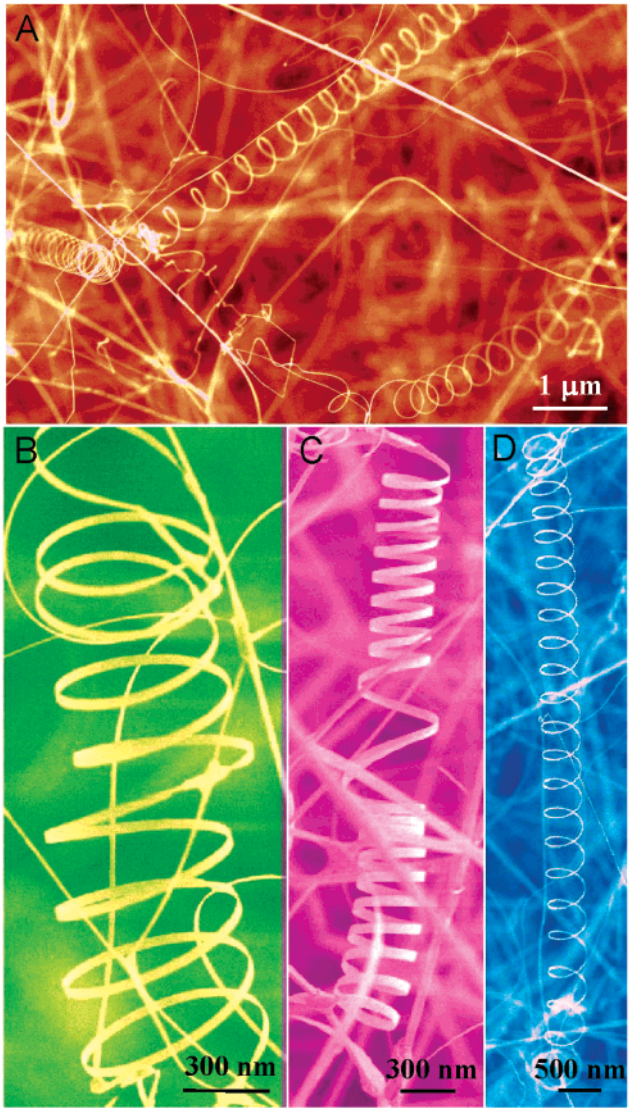

Figure 3. SEM images of the as-synthesized ZnO nanobelts, showing helical nanostructure. The typical width of the nanobelt is ~30 nm, and pitch distance is rather uniform. The helixes are right-handed.

density (σ) is preserved before and after rolling, because the surface charges are intrinsic ionic charges owing to the unique crystallographic structure of ZnO rather than the induced charges that could "freely" flow. The change in electrostatic energy is calculated as the difference of electrostatic energies between the cylinder and the plate,[31] which is

$$\Delta E_{\text{electro}} \approx -\frac{\pi W \sigma^2}{\epsilon \epsilon_0} t^2 \qquad (1)$$

where ϵ is the dielectric constant. Based on elasticity theory, the elastic energy stored in a uniform cylinder is[32]

$$\Delta E_{\text{elastic}} \approx \frac{\pi W Y}{24 R} t^3 \qquad (2)$$

where Y is the bending modulus of the nanobelt. Therefore,

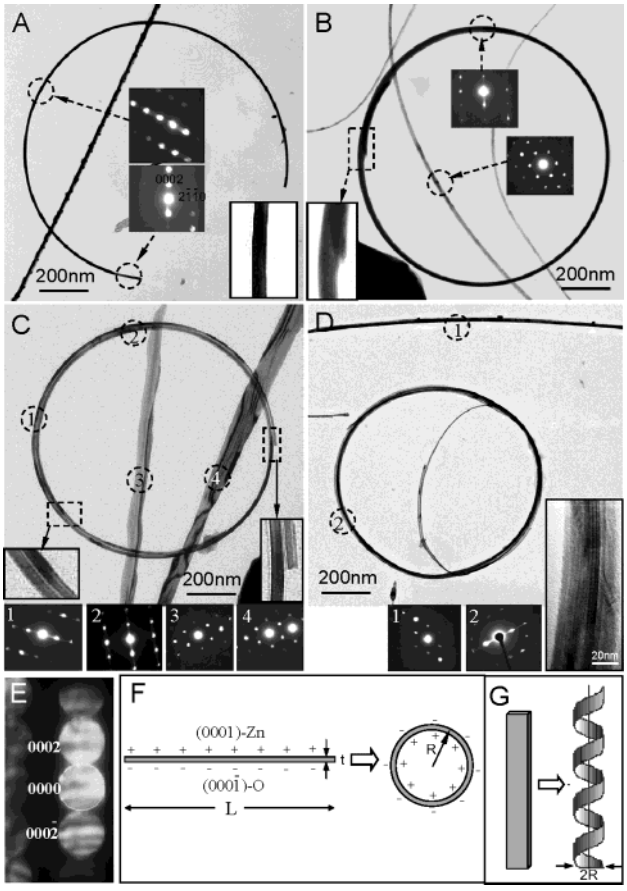

Figure 4. (A,B,C,D) TEM images and the corresponding electron diffraction patterns recorded from the regions marked in the figure from an incomplete ring, a single-looped ring, double-looped ring, and multiple-looped ring, respectively, without tilting the specimen. Enlarged images from the nanobelts are inserted, from which the number of loops and the contact between the nanobelts can be directly imaged. Electron diffraction patterns recorded from the nanorings prove unanimously that the normal direction of the circular ring plane is [01$\bar{1}$0], and the [0001] *c*-axis is pointing to the ring center and it rotates following the arc of the ring. Electron diffraction patterns recorded from the straight nanobelts or closely straight nanobelts are [0001] pattern, in consistent to the results presented in Figure 2(A,B). (E) Convergent beam electron diffraction from a nanobelt, showing the polarity of the nanobelt as evidenced by the asymmetric intensity distribution in the (0002) and (000$\bar{2}$) disks. The result shows that the interior of the nanoring is positive charged and the exterior is negatively charged. (F) A schematic model of a nanobelt as viewed parallel to its flat surfaces, displaying the ±(0001) polar surfaces with a macroscopic dipole moment; a closed ring structure of the nanobelt, showing the neutralized dipole moment with lower electrostatic energy but higher elastic energy. The stable shape is created to minimize the total energy contributed by polarization and elasticity. (G) Schematic models showing the formation of helical nanostructures by rolling up a nanobelt.

the change in total energy is

$$\Delta E \approx -\frac{\pi W \sigma^2}{\epsilon \epsilon_0} t^2 + \frac{\pi W Y}{24 R} t^3 \qquad (3)$$

From eq 3, there exists a critical thickness-to-radius ratio

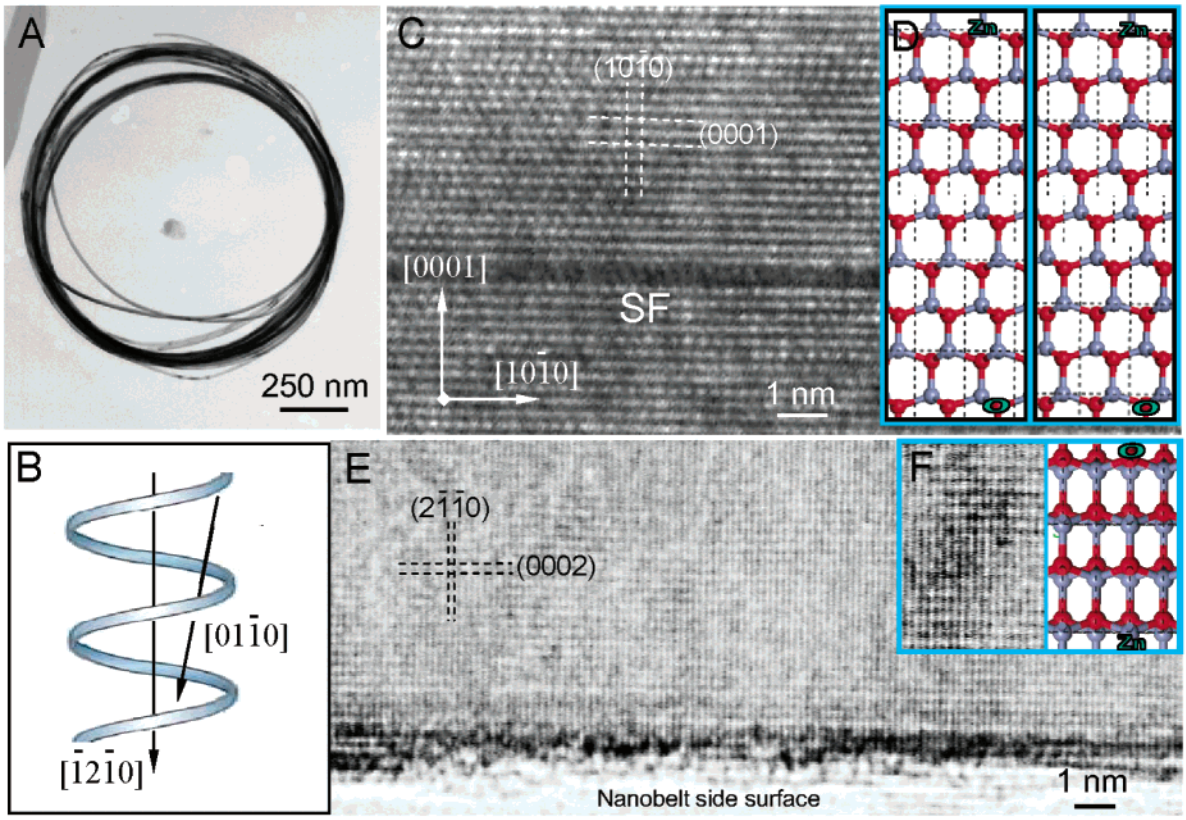

Figure 5. (A) TEM image of a helical nanostructure formed by multiple-loop rolling up of a nanobelt. (B) Schematic model showing the relative orientation for recording high-resolution TEM images along the axial direction of the helical nanostructure ([$\bar{1}$2$\bar{1}$0]), and the [01$\bar{1}$0] perpendicular to the nanobelt and parallel to its polar surface. (C) [$\bar{1}$2$\bar{1}$0] high-resolution TEM image of a nanobelt showing the dislocation-free volume but with the presence of stacking faults (SFs). (D) Two possible atomic models in correspondence to the HRTEM image given in (C), showing that stacking fault has no effect on the polarity of the nanobelt. (E) [01$\bar{1}$0] high-resolution TEM image of a nanobelt and the profile of its side surface, showing dislocation-free volume. (F) An enlargement of the image given in (E) and the projected atomic structure model.

$(t/R)^*$, at which $\Delta E = 0$,

$$\alpha \equiv \left(\frac{t}{R}\right)^* = \frac{24\sigma^2}{\epsilon\epsilon_0 Y} \tag{4}$$

where $\Delta E < 0$ if $t/R < \alpha$, and $\Delta E > 0$ if $t/R > \alpha$. The bending modulus for free-standing nanobelts has been measured by the mechanical resonance[22] and nanoindentation[33] techniques to be $Y = 50 \pm 5$ GPa, $\epsilon = 4.6$,[34] and surface charge density $|\sigma| = 0.057$ C/m^2 based on the first principle calculation.[24,30]. Equation 4 gives $\alpha = (3.8 \pm 0.2) \times 10^{-2}$. Measurements from Figures 4A, B, and C give $t/R = (2.0 \pm 0.1) \times 10^{-2}$, $(3.1 \pm 0.1) \times 10^{-2}$, and $(2.8 \pm 0.1) \times 10^{-2}$, respectively, all of which are smaller than the α value from eq 4; thus, the nanoring structure is energetically favorable. For a nanoring of typical radius of $R = 400$ nm as observed in Figure 1, eq 4 gives $t^* \approx 15$ nm. Therefore, if the thickness of the nanobelt is smaller than 15 nm, the total energy ΔE drops after forming a ring, suggesting that the ring configuration may be the preferred shape; while for thicker nanobelts, the straight configuration is the stable shape. The formation of the helical structure as shown in Figure 3 is the simultaneous rolling of the nanobelt while it continues to grow along the *a*-axis (Figure 4G).

The atomic structure of the nanobelt has been investigated by HRTEM. The model for the helical nanostructure shown in Figure 5A is given in Figure 5B. We have chosen two orientations to investigate the atomic structure of the helical nanostructure. The first orientation is along the axis of the helical nanostructure, which is [$\bar{1}$2$\bar{1}$0], and the second orientation [01$\bar{1}$0] is parallel to the top (0001) surface and perpendicular to the side surface of the nanobelt. The HRTEM image recorded along [$\bar{1}$2$\bar{1}$0] shows clearly the (10$\bar{1}$0) ($d = 0.28$ nm) and (0002) ($d = 0.26$ nm) fringes without the presence of dislocation, but stacking faults parallel to the (0001) plane are identified. The stacking fault is extrinsic with insertion of an extra Zn−O layer parallel to the basal plane. The most important result is that *the presence of (0001) stacking faults does not affect the polarity of ZnO*, as shown by the models in Figure 5D. The HRTEM image recorded along [01$\bar{1}$0] clearly presents the (0002) ($d = 0.26$ nm) and (2$\bar{1}\bar{1}$0) ($d = 0.16$ nm) fringes (Figure 5E). An enlarged image and the projected atomic structural model are given in Figure 5F, which also preserve the polarity. The top surface of the nanobelt is flat with the presence of a few atom-height steps as displayed by the profile image in Figure 5E.

The growth of polar facet-dominated nanobelt surfaces is a major step toward development of piezoelectric and ferroelectric one-dimensional nanostructures. Because the ZnO (2$\bar{1}\bar{1}$0) plane has a surface energy lower than that of

either (0001) or (01$\bar{1}$0), a fast growth along [2$\bar{1}\bar{1}$0] (*a*-axis) to form a nanobelt structure may be unfavorable from the energy point of view. But the success of controlled growth of free-standing (0001) polar-surface-dominated nanobelts along the *a*-axis demonstrates the experimental feasibility of overcoming the energy barrier through growth kinetics, thus providing a feasible approach for growing structurally controlled nanobelts of technological importance.

Helical structure is the most fundamental structural configuration for DNA and many biological proteins, which is due to van der Waals force and hydrogen bonding. For one-dimensional nanostructures, nanocoils and nanorings have been observed for carbon nanotubes[35−37] and SiC,[38] the former are created due to a periodic arrangement of the paired pentagon and heptagon carbon rings in the hexagonal carbon network,[39] and the latter are due to stacking faults and twins. These helical structures are produced by the presence of point or planar defects (twins and stacking faults). The striking new feature of the helical nanostructures for single crystalline ZnO nanobelt reported here is that they are the spontaneous polarization induced structures.[40] The nanobelts and helical nanostructures are an ideal system for understanding piezoelectricity and polarization-induced ferroelectricity at nanoscale. Quantitative analysis about the elastic energy involved in the formation of helical structure could provide an experimental measurement on the electrostatic energy induced by spontaneous polarization, leading to a possible technique for measuring the dipole moment and surface charge distribution in nanobelt structures. The different polar surfaces could be used as selective catalysts. The piezoelectric and ferroelectric nanobelt structures may open up many research possibilities and applications at the nanoscale, such as nanoinductors, nanospring-based transducers and actuators, and tunable functional components for MEMS and NEMS. The tunable pitch distance in the helical nanosprings could be used for separating DNA double helix chains and tailoring DNA structures via electromechanical coupling.[41]

Note Added after ASAP Posting. This article was posted ASAP on 8/6/2003. Changes have been made in the Abstract, the caption to Figure 3, and Figure 4. The correct version was posted on 8/18/2003.

References

(1) Minne, S. C.; Manalis, S. R.; Quate, C. F. *Appl. Phys. Lett.* **1995**, *67*, 3918.
(2) See the special issue on transparent conducting oxides, *MRS Bulletin*, August issue, **2000**.
(3) Gorla, C. R.; Emanetoglu, N. W.; Liang, S.; Mayo, W. E.; Lu, Y.; Wraback, M.; Shen, H. *J. Appl. Phys.* **1999**, *85*, 2595.
(4) Dulub, O.; Boatner, L. A.; Diebold, U. *Surf. Sci.* **2002**, *519*, 201.
(5) Meyer, B.; Marx, D. *Phys. Rev. B* **2003**, *67*, 035403.
(6) Tasker, P. W. *J. Phys. C: Solid State Phys.* **1979**, *12*, 4977.
(7) Dulub, O.; Diebold, U.; Kresse, G. *Phys. Rev. Lett.* **2003**, *90*, 016102-1.
(8) Wander, A.; Schedin, F.; Steadman, P.; Norris, A.; McGrath, R.; Turner, T. S.; Thornton, G.; Harrison, N. M. *Phys. Rev. Lett.* **2001**, *86*, 3811.
(9) Staemmler, V.; Fink, K.; Meyer, B.; Marx, D.; Kunat, M.; Gil, G. S.; Burghaus, U.; Woll, Ch. *Phys. Rev. Lett.* **2003**, *90*, 106102-1.
(10) Cui, Y.; Lieber, C. M. *Science* **2001**, *291*, 851.
(11) Huang, Y.; Duan, X. F.; Cui, Y.; Lauhon, L. J.; Kim, K. H.; Lieber, C. M. *Science* **2001**, *294*, 1313.
(12) Collins, P. C.; Arnold, M. S.; Avouris, Ph. *Science* **2001**, *292*, 706.
(13) Bachtold, A.; Hadley, P.; Nakanishi, T.; Dekker, C. *Science* **2001**, *294*, 1317.
(14) Ma, D. D. D.; Lee, C. S.; Au, F. C. K.; Tong, S. Y.; Lee, S. T. *Science* **2003**, *299*, 1874.
(15) Duan, X. F.; Huang, Y.; Agarwal, R.; Lieber, C. M. *Nature* **2003**, *421*, 241.
(16) Wang, Z. L., Ed.; *Nanowires and Nanobelts, Vol. I: Metals and Semiconductor Nanowires; Vol. II: Nanowires and Nanobelts of Functional Materials*; Kluwer Academic Publisher: New York, 2003.
(17) Huang, M. H.; Mao, S.; Feick, H.; Yan, H.; Wu, Y.; Kind, H.; Weber, E.; Russo, R.; Yang, P. *Science* **2001**, *292*, 1897.
(18) Pan, Z. W.; Dai, Z. R.; Wang, Z. L. *Science* **2001**, *291*, 1947.
(19) Arnold, M.; Avouris, Ph.; Pan, Z. W.; Wang, Z. L. *J. Phys. Chem. B* **2002**, *107*, 659.
(20) Comini, E.; Faglia, G.; Sberveglieri, G.; Pan, Z. W.; Wang, Z. L. *Appl. Phys. Lett.* **2002**, *81*, 1869.
(21) Hughes, W. L.; Wang, Z. L. *Appl. Phys. Lett.* **2003**, *82*, 2886.
(22) Bai, X. D.; Wang, E. G.; Gao, P. X.; Wang, Z. L. *Appl. Phys. Lett.* **2003**, *82*, 4806.
(23) Corso, A. D.; Posternak, M.; Resta, R.; Baldereschi, A. *Phys. Rev. B* **1994**, *50*, 10715.
(24) Bernardini, F.; Fiorentini, V.; Vanderbilt, D. *Phys. Rev. B* **1997**, *56*, 10024. The theoretically calculated piezoelectric coefficients for ZnO are: $\epsilon 33 = 0.89$, $\epsilon 31 = -0.51$ C/m^2. The experimentally measured $\epsilon 33 = 1.0-1.2$ C/m^2.
(25) Wang, Z. L.; Kong, X. Y. Patent pending, Georgia Tech, 2003.
(26) Kohl, D.; Henzler, M.; Heiland, G. *Surf. Sci.* **1974**, *41*, 403.
(27) The as-synthesized samples were characterized by field emission source scanning electron microscopy (SEM) (LEO 1530 FEG at 5 kV), high-resolution transmission electron microscopy (HRTEM) (Hitachi HF-2000 FEG at 200 kV and JEOL 4000EX at 400 kV).
(28) Vigue, F.; Vennegues, P.; Vezian, S.; Laugt, M.; Faurie, J.-P. *Appl. Phys. Lett.* **2001**, *79*, 194.
(29) The polarity of ZnO results in asymmetric intensity distribution in the (0002) and (000$\bar{2}$) diffraction disks. The polarity was determined by comparing the experimentally observed convergent beam electron diffraction pattern with the theoretically calculated diffraction pattern. Details of the calculation can be found in Spence, J. C. H.; Zuo, J. M. *Electron Microdiffraction*; Plenum Press: New York, 1992.
(30) The local deposition temperature is ∼400−500 °C, which is high enough to prevent physical adsorption of molecules on the surface during the growth. Thus, the ionic charges on the surface are likely uncompensated and are electrostatically effective for producing the helical structure.
(31) The calculation was made based on following approximations: [1] the thickness of the nanobelt is much smaller than the radius of the nanoring ($t \ll R$); [2] the width (W) of the nanobelt is significantly larger than its thickness, so that the edge effect is small. However, it is the difference between the electrostatic energy before and after rolling into a cylinder that matters to the final result; if the edge effect before and after rolling is preserved, the edge effect, if any, is almost canceled out in the final equation. [3] The surface charges are due to the unique crystallographic structure of ZnO, and they are bound to the atoms, thus, the surface charge density is preserved after rolling into a cylinder. Therefore, the total charge on the inner surface of the cylinder is $Q = 2\pi(R - t/2)W\sigma$. The change in electrostatic energy is

$$\Delta E_{\text{electro}} = \frac{\pi W\sigma^2 R^2}{\epsilon\epsilon_0}\left[(1-\beta)^2 \ln\left(\frac{1+\beta}{1-\beta}\right) - 2\beta\right] \approx -\frac{\pi W\sigma^2}{\epsilon\epsilon_0} t^2 \quad (\text{for } t \ll R)$$

where $\beta \equiv t/2R$.
(32) Because the thickness of the nanobelt is very small and the ring radius is large, the radial stress across the nanobelt is negligible because the two sides are free surfaces without external force. The strain along the *z*-direction (the axis of the cylinder) is also zero because there is no twisting. The only strain is along the ϕ-direction. The elastic energy is the volume integration of the ϕ-direction strain energy. The bending modulus used for the calculation was based on the experimentally measured value for ZnO nanobelts with inclusion of geometrical factor.
(33) Mao, S.; Zhao, M.; Wang, Z. L. *Appl. Phys. Lett.*, submitted.
(34) Bernardini, F.; Fiorentini, V. *Phys. Rev. B* **1998**, *58*, 15292.
(35) Amelinckx, S.; Zhang, X. B.; Bernaerts, D.; Zhang, X. F.; Ivanov, V.; Nagy, J. B. *Science* **1994**, *265*, 635.
(36) Martel, R.; Shea, H. R.; Avouris, Ph. *Nature* **1999**, *398*, 299.
(37) Sano, M.; Kamino, A.; Okamura, J.; Shinkai, S. *Science* **2001**, *293*, 1299.

(38) Zhang, H.-F.; Wang, C.-M.; Wang, L.-S. *Nano Lett*. **2002**, *2*, 941.
(39) Gao, R. P.; Wang, Z. L.; Fan, S. S. *J. Phys. Chem. B* **2000**, *104*, 1227.
(40) In-situ heating of the helical nanostructure has been carried out in TEM under vacuum of 10−8 Torr. Heating the specimen to 400 °C generated a high concentration of oxygen vacancies based our previous study in ref. 19, but no visible change in the shape of the helical nanostructure was found, suggesting that the role played by point defects in the formation of helical structure is undetectable.
(41) Thanks the support from NSF and NASA URETI. Thanks to Profs. Min Zhou and Ashok Saxena for discussion.

NL034463P